Results in Physics 67 (2024) 108057

Contents lists available at ScienceDirect

Results in Physics

journal homepage: www.elsevier.com/locate/rinp

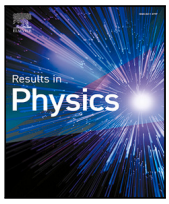

Nonreciprocal spin wave channeling in ferromagnetic/heavy-metal nanostrips

R.A. Gallardo [a,*], P. Alvarado-Seguel [b], F. Brevis [a], C. Gonzalez-Fuentes [c], J.W. González [d], K. Lenz [e], J. Lindner [e], A. Roldán-Molina [f]

[a] Departamento de Física, Universidad Técnica Federico Santa María, Avenida España 1680, Valparaíso, Chile
[b] Departamento de Matemáticas, Universidad de Chile, Las Palmeras 3425, Ñuñoa, Santiago, Chile
[c] Instituto de Física, Pontificia Universidad Católica de Chile, icuña Mackena 4860, 7820436 Santiago, Chile
[d] Departamento de Física, Universidad de Antofagasta, Av. Angamos 601, Casilla 170, Antofagasta, Chile
[e] Helmholtz-Zentrum Dresden-Rossendorf, Institute of Ion Beam Physics and Materials Research, Bautzner Landstraße 400, 01328 Dresden, Germany
[f] Universidad de Aysén, Calle Obispo Vielmo 62, Coyhaique, Chile

ARTICLE INFO

Keywords:
Spin waves
Nonreciprocity
Spin wave channeling
Chiral interaction

ABSTRACT

Nonreciprocity, unidirectionality, and channeling are essential concepts for potential magnonic applications. Nonreciprocity and unidirectionality ensure the efficient propagation of spin waves along predetermined paths with preferential directions, disrupting the symmetry of counterpropagating waves. Channeling fosters the development of intricate spin-wave networks, enabling more sophisticated functionalities. Integrating these concepts into practical applications will shape the future of spin-wave-based information processing devices. This article theoretically studies the dynamics of spin waves in a ferromagnetic strip coupled to a heavy-metal strip, where the nonreciprocity, unidirectionality, and channeling effects are analyzed. Both backward volume (BV) and Damon–Eshbach (DE) configurations are considered, where the lateral dimensions of the heavy-metal and ferromagnetic strips can differ. Calculations show notable nonreciprocal channeling of spin waves in both DE and BV modes. In the BV configuration, the dispersion is reciprocal with nontrivial localization of lateral confined modes. It is shown that the waves can be channeled into the zones in contact with the HM, where the Dzyaloshinskii–Moriya interaction is active. In the DE configuration, the waves exhibit nonreciprocal spin-wave dispersion, allowing unidirectional and channeled spin-wave propagation. The main results are compared to micromagnetic simulations, where an excellent agreement between both methods is obtained. These findings are relevant for envisioning advanced magnonic devices, enabling precise control over spin-wave propagation for innovative, low-power, high-speed information processing.

Introduction

The guided propagation of spin waves (SWs) through nanoscale conduits is crucial for developing magnonic devices with technological significance [1,2]. These waves, which encode information in their amplitude and phase, are considered promising candidates due to their low power consumption, high speed, and broad application spectrum spanning from the MHz to THz frequencies [3,4]. While SWs can be guided through narrow magnetic elements, roughness and imperfections along the sample's edges may affect efficient energy propagation. One approach to mitigate wave scattering induced by edge imperfections is to utilize a domain wall as a waveguide. In this scenario, the effective internal field exhibits a minimum within the wall center, creating a potential well for the spin waves, analogous to the index gradient in optical fibers for light [1,2,5–7]. Another route toward robust spin-wave conduction in narrow pathways involves spin-wave channeling in magnetization-graded nanostructures [8,9], where the modification of the magnetic properties allows for the localized propagation of SWs in narrow nanometric zones. Such SW channeling is essential for the miniaturization of magnonic devices.

In addition to channeling spin waves, it is also important to add nonreciprocal characteristics to such waves, whose properties can be exploited to generate magnonic logic devices [10,11]. In recent years, there has been a growing interest in studying spin waves in magnetic systems exhibiting chiral features [12–14]. One of the prominent interactions that induce chirality is the antisymmetric Dzyaloshinskii–Moriya interaction (DMI) [15–17], which emerges in noncentrosymmetric crystals [18–20] and ultrathin ferromagnetic films coupled to a heavy-metal layer [21–23]. A significant asymmetry in the spin-wave

* Corresponding author.
E-mail address: rodolfo.gallardo@usm.cl (R.A. Gallardo).

https://doi.org/10.1016/j.rinp.2024.108057
Received 26 September 2024; Received in revised form 12 November 2024; Accepted 20 November 2024
Available online 27 November 2024

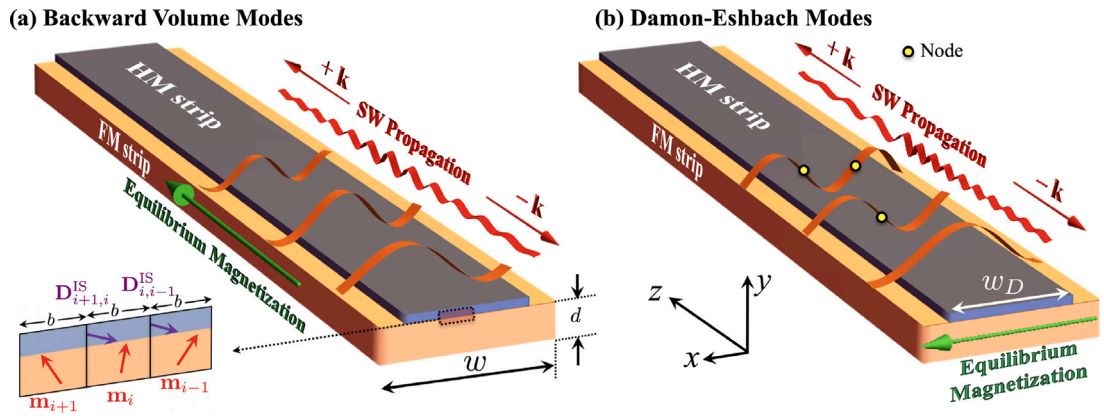

Fig. 1. Illustration of a ferromagnetic thin strip of width w and thickness d. The ferromagnetic nanostructure is coupled with a heavy-metal (HM) strip of width w_D. (a) shows the backward-volume configuration, where both the equilibrium magnetization and the spin-wave propagation are along the z-axis. In this configuration, the interfacial nature of the DMI induces an interaction among the lateral spins that modifies the nature of the lateral confined waves. In contrast, the DM coupling of the spins along z is null. In (b), the Damon–Eshbach geometry is illustrated with the equilibrium magnetization pointing along x. Nonreciprocal spin waves propagate along z due to DMI, while the lateral spins do not experience Dzyaloshinskii–Moriya coupling.

dispersion is observed in systems with DMI [12–14,18,24,25], where two counterpropagating waves exhibit different wavelengths at the same frequency. Under specific conditions, the classical dipole–dipole interaction behaves as a DMI-like mechanism, inducing magnetochiral effects on magnons. Such chiral effects have been observed in curvilinear shells [26–28], and planar systems, such as magnetization-graded ferromagnetic films [8], ferromagnetic bilayers [29–38], and bilayered magnonic crystals [39,40]. With this nonreciprocity property, a wave can even be suppressed in one direction while the counterpropagating one remains unaffected. This unidirectionality is essential for various magnonic logic devices such as circulators, isolators, phase shifters, and magnonic diodes [20,41–47].

The exploration of nanostructures exhibiting nonreciprocal and channeling effects is of great significance in the field of magnonics. This article presents a theoretical study, based on the dynamic matrix model, of spin-wave dynamics in a thin ferromagnetic strip coupled with a heavy-metal strip, examining scenarios where the strips can have different widths. Both backward volume (BV) and Damon–Eshbach (DE) configurations are investigated to elucidate the conditions that lead to spin-wave unidirectionality, channeling, and nonreciprocity. In the BV configuration, significant modifications in spin-wave profiles are observed, resulting in a nontrivial spatial evolution of lateral confined waves. The BV modes display symmetric dispersion, with the low-frequency mode being channeled into regions in contact with the heavy-metal layer under a significant Dzyaloshinskii–Moriya interaction. In contrast, the DE configuration exhibits asymmetric spin-wave dispersion, where unidirectional waves are prominent. Comparative analysis with micromagnetic simulations shows an excellent agreement between both methods, validating the theoretical model. This study emphasizes the potential for designing advanced magnonic devices by leveraging the unique properties of nonreciprocal and channeled spin waves in nanometric systems, paving the way for innovative applications in low-power, high-speed information processing technologies.

Model

Dynamic matrix method

The theoretical calculations of the spin-wave dynamics in ferromagnetic strips are based on Ref. [9], where the propagating waves and standing SW modes were studied in a finite magnetization-graded ferromagnetic strip. The dynamic matrix method (DMM) was used to account for the spatial variation of the dynamic magnetization along the strip width. This method involves splitting the strip into many sub-strips (discretization along the x axis) that interact via dipolar, DMI and exchange coupling, allowing for the local modification of magnetic properties in each sub-strip. By following Ref. [9], the magnetization dynamics of each sub-strip are modeled by the Landau–Lifshitz equation $\dot{\mathbf{M}}^n(\mathbf{r},t) = -\gamma \mathbf{M}^n(\mathbf{r},t) \times \mathbf{H}^n(\mathbf{r},t)$, with $\mathbf{M}^n(\mathbf{r},t)$ being the magnetization and $\mathbf{H}^n(\mathbf{r},t)$ the effective field. Both fields, magnetization and effective field, are written in terms of static (zeroth order) and dynamic (first-order) components, namely $\mathbf{M}^n(\mathbf{r},t) = \mathbf{M}^n_{\text{eq}} + \mathbf{m}^n e^{i(kz-\omega t)}$ and $\mathbf{H}^n(\mathbf{r},t) = \mathbf{H}^n_{\text{eq}} + \mathbf{h}^n e^{i(kz-\omega t)}$. Thus, the equation of motion can be written as

$$\omega \mathbf{m}^n = i\gamma(\mathbf{H}^n_{\text{eq}} \times \mathbf{m}^n + \mathbf{h}^n \times \mathbf{M}^n_{\text{eq}}), \tag{1}$$

where the higher-order terms have been omitted. Then, by writing $\mathbf{h}^n = -\sum_p \Lambda^{np} \cdot \mathbf{m}^p$, an eigenvalue problem of the form $\bar{\mathbf{T}}\mathbf{m} = \omega \mathbf{m}$ is obtained. Therefore, once the dynamic fields $\mathbf{h}^n$ (or Λ^{np}) and static effective fields $\mathbf{H}^n_{\text{eq}}$ are derived, the matrix $\bar{\mathbf{T}}$ is obtained, which allows for calculating the dispersion relation ($\omega(k)$) and dynamic magnetization components (coefficients $\mathbf{m}^n$) of the system. Note that the effective field contains the contribution of the external field, as well as exchange and dipolar interaction between sub-strips. Due to the complexity that involves the calculations of dipolar interactions, it is assumed that the magnetization and the external field are fully parallel. Besides, the dynamic magnetization components are assumed to be uniform along the normal direction, which applies to the current system because the strip is ultrathin. With these considerations, it is feasible to calculate the static and dynamic dipolar and exchange fields, as shown in appendices B and C of Ref. [9]. For the case of the dipolar interaction, the calculations are based on the idea that the cross-section of the strips is small enough so that the stray fields generated by a sub-trip p can be averaged into the strip n and vice versa. Thus, the static demagnetizing field and dynamic dipolar interaction are fully considered in theory (see Ref. [9] for further details).

In the current work, an interfacial DMI is included, which is activated by coupling a heavy-metal (HM) layer above the ferromagnetic (FM) strip, as depicted in Fig. 1. Due to the fact that the DMI coupling depends on the equilibrium magnetization configuration [12,13], the effective Dzyaloshinskii–Moriya fields for DE and BV configurations require to be analyzed separately.

In the case of backward-volume waves, the equilibrium magnetization and SW propagation are along the strip axis (z). Hence, the DMI is active for laterally interacting magnetic moments, as shown in the inset of Fig. 1(a), while for the spins interacting along z (along the strip) the DM coupling is null [12]. Therefore, it can be anticipated that the confined modes along the strip's width will be modified by the DMI, while the spin waves propagating along the long strip axis will not.

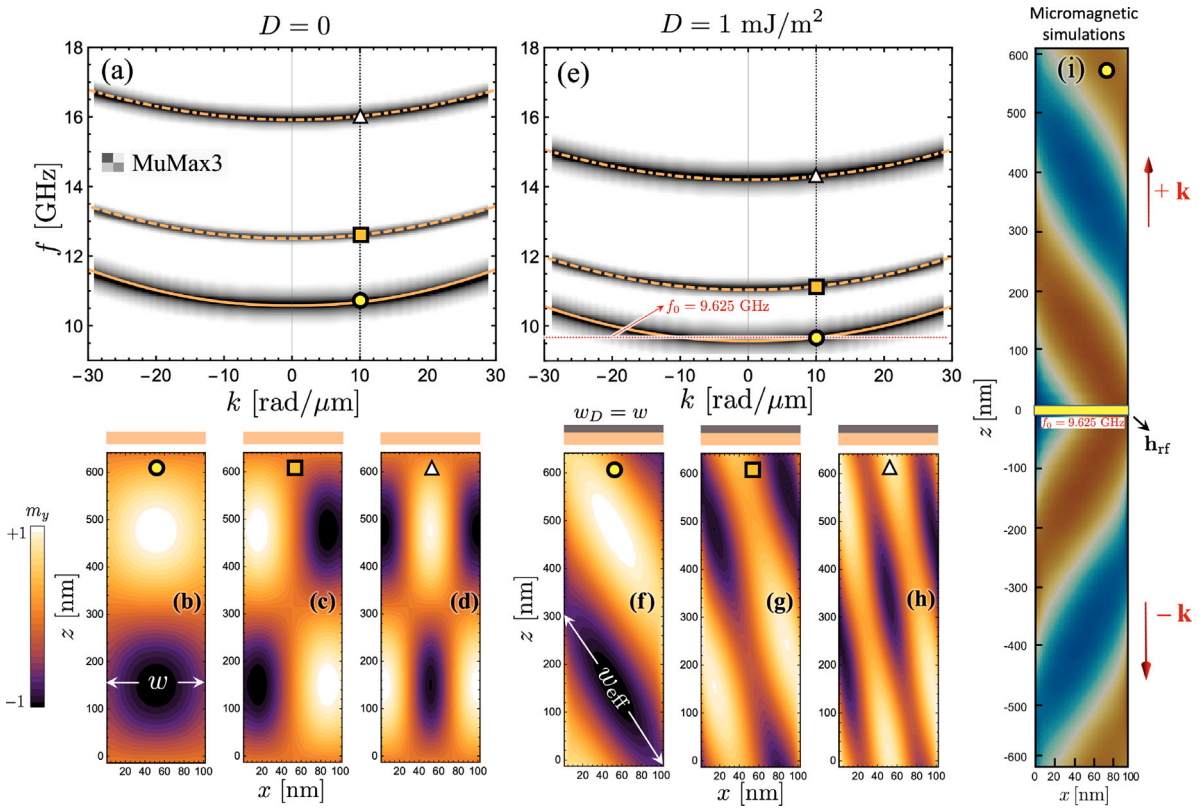

Fig. 2. SW dynamics calculated at $w = w_D = 100$ nm for the backward-volume configuration. (a) illustrates the SW dispersion and (b–d) the magnetization profiles with $D = 0$. (e) shows the SW dispersion and (f–h) the magnetization profiles calculated for $D = 1$ mJ/m^2. In (a) and (e), the lines correspond to the SW dispersion obtained from the DMM, while the grayscale corresponds to the simulated results. The profiles in (b–d) and (f–h) are obtained for the DMM calculations that consider the normalized dynamic magnetization component m_y (real part), which is evaluated in arbitrary units. The simulated magnetization profile of the low-frequency mode, evaluated at $D = 1$ mJ/m^2 and $f_0 = 9.625$ GHz, is illustrated in (i). The strip width w, and effective width w_{eff} for the cases $D = 0$ and $D = 1$ mJ/m^2 are shown in (b) and (f), respectively.

Thus, reciprocal spin-wave dispersion is expected along z, as depicted schematically in Fig. 1(a). As shown in Appendix, the dynamic effective field components acting in the ith strip are

$$\left(h_x^{\text{IS}}\right)_i = \frac{D}{\mu_0 M_s^2 b} \sum_\nu m_y^{(\nu)} \left(\delta_\nu^{i+1} - \delta_\nu^{i-1}\right), \tag{2}$$

and

$$\left(h_y^{\text{IS}}\right)_i = -\frac{D}{\mu_0 M_s^2 b} \sum_\nu m_x^{(\nu)} \left(\delta_\nu^{i+1} - \delta_\nu^{i-1}\right), \tag{3}$$

where δ_j^i stands for the Kronecker delta symbol, D is the DM constant, and M_s the saturation magnetization. IS refers to the inter-stripe Dzyaloshinskii–Moriya interaction.

For the Damon–Eshbach configuration, the equilibrium magnetization is along x, and the dynamic magnetization oscillates in the y-z plane. The DM interaction between sub-strips along the strip width (x-direction) is zero and, therefore, the effective field DM components are simply given by [13,48]

$$\left(h_z^{\text{DM}}\right)_i = \frac{2ikD}{\mu_0 M_s^2} m_y^{(i)}, \tag{4}$$

and

$$\left(h_y^{\text{DM}}\right)_i = -\frac{2ikD}{\mu_0 M_s^2} m_z^{(i)}, \tag{5}$$

with k being the wave vector. In Eqs. (4) and (5), the field and dynamic magnetization components have the same indices i, which means the intra-strip nature of the DM for the DE modes, so there is no Dzyaloshinskii–Moriya interaction between two different sub-strips. Therefore, the confined modes along the strip width will behave in the same manner as the typical standing waves in a non-chiral geometrically confined system. Nevertheless, the waves propagating along the strip will be influenced by the DM interaction, inducing an asymmetry in the spin-wave dispersion, as will be discussed in the following section. The Zeeman, dipolar, and exchange interactions are also considered, where the details of the effective fields associated with these energies are described in Ref. [9].

Micromagnetic simulations

Micromagnetic simulations were performed by using the GPU-accelerated code MuMax3 [49,50]. The ferromagnetic stripe was simulated with size 2^{15} nm $\times\, w \times 1$ nm with cell sizes 2 nm $\times$ 2 nm $\times$ 1 nm along the z, x, y components, respectively. A central region with width w_D was defined where the DMI strength $D \geq 0$ and $w_D \leq w$. Periodic boundary conditions along the z-direction were applied in order to minimize the effect of the spin waves reflections. For BV(DE) configuration, the system was initialized with a magnetization along the $z(x)$-direction and a magnetic field was applied along this component to saturate the sample. All the parameters are the same as considered for the theoretical calculation for each case. The generation of spin waves was implemented through an applied space–time dependent pulse. Since the excited spin-wave modes depend on the spatial shape of the pulse, an arbitrary fully asymmetric function along the width was considered in order to obtain the full spin-wave dispersion. This function is given by $\mathbf{h}_{\text{rf}} = h_0\,\text{sinc}\left[2\pi f_c(t-t_0)\right] \times \text{sinc}\left(k_z z\right) \times \mathcal{A}(x)\,\hat{y}$ at the center of the sample with h_0 ten times smaller than the field used to saturate the sample. The cut-off frequency was $f_c = 30$ GHz and $t_0 = 49.99$ ps. Besides, $k_z = 2\pi/\lambda$ where $\lambda = 20$ nm, $\mathcal{A}(x) = \tanh(k_x x + \psi)$, $k_x = 3 \cdot 10^7$ nm^{-1} and $\psi = 1.0$. The system evolved for 20 ns and the magnetization was stored every 0.5 ps. The dispersion relation was obtained by calculating the two-dimensional fast Fourier transform in time and space of the stored data by using the Python library OOMMFPy [51] and the micromagnetic simulation environment Ubermag [52]. To simulate arbitrary modes at

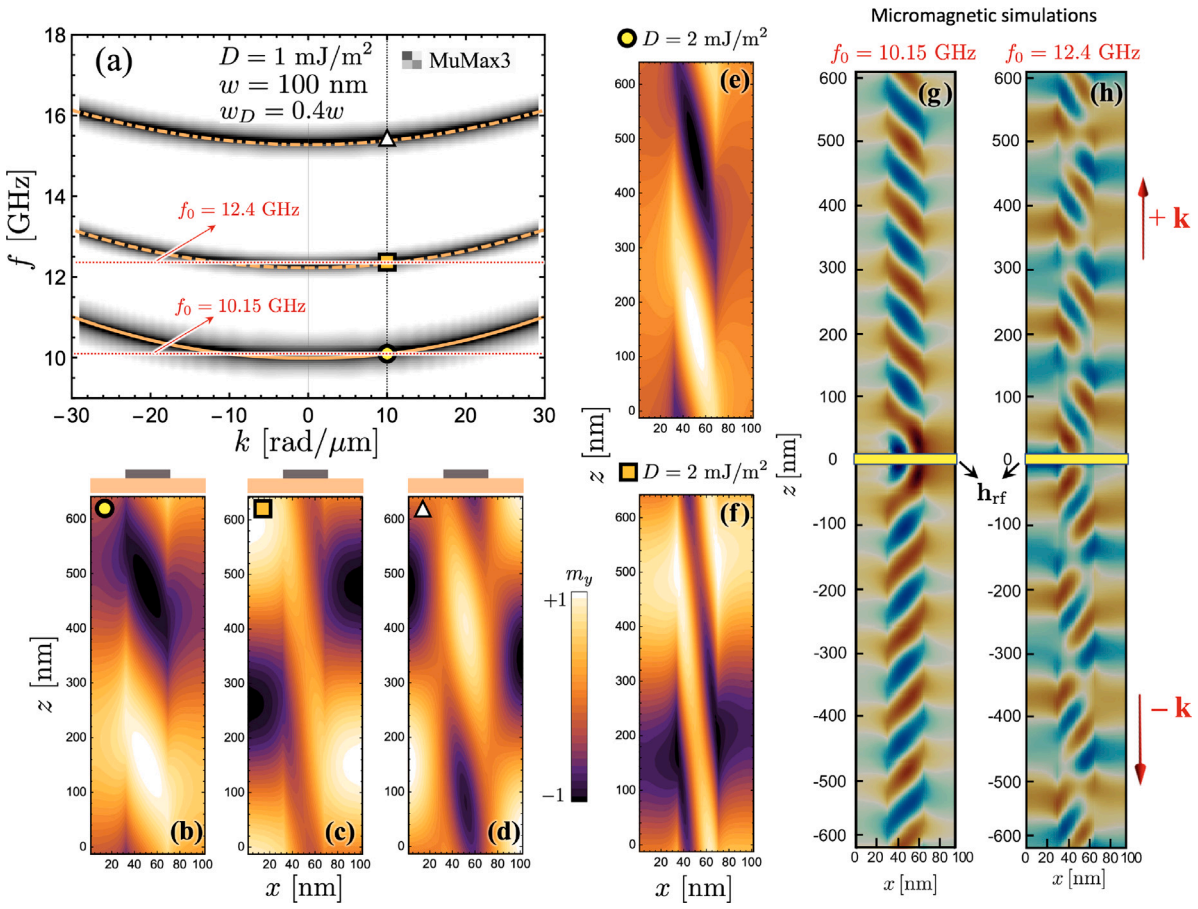

Fig. 3. (a) lines (grayscale) show the calculated (simulated) dispersion relation for the case $D = 1$ mJ/m^2 and $w_D = 0.4w$, with $w = 100$ nm. (b)–(d) depict the real part of the magnetization profiles evaluated at $k = +10$ rad/μm. A hybridized confinement character along the strip width is observed in the system, which is enhanced for $D = 2$ mJ/m^2, as shown in (e) and (f). The cases (b–f) have been calculated with the DMM. Simulated SW profiles are shown in (g) and (h), which are consistent with the calculated cases (e) and (f), respectively.

a certain frequency f_0, a pulse of the following type was considered $\mathbf{h}_{rf} = h_0 \sin\left[2\pi f_0(t - t_0)\right] \times \mathrm{sinc}\left(k_z z\right) \times \mathcal{A}(x)\,\hat{y}$. For symmetric modes, $\mathcal{A}(x)$ was set to 1.

Results and discussion

The spin-wave spectra will be studied for backward-volume and Damon–Eshbach configurations. In the case of DE geometry, an in-plane external field of $\mu_0 H = 100$ mT is applied along the strip width so that the equilibrium magnetization is assumed to be fully saturated along the x axis. For the BV configuration, a small external field is enough to saturate the sample at $D = 0$ because no magnetic charges are formed in the lateral strip edges. Nevertheless, as the DM constant D increases, the texture formation driven by the DMI could make the saturated state unstable. Hence, for BV modes, a bias field of $\mu_0 H = 100$ mT is also applied along the z axis. The assumption of saturated states under an external field of $\mu_0 H = 100$ mT was verified using micromagnetic simulations, which showed small spin deviations of approximately 1% at the strip edges in the DE configuration and a practically saturated state for BV geometry. With respect to the magnetic parameters, a permalloy sample ($Ni_{80}Fe_{20}$) is used as a reference so that the saturation magnetization and exchange constant are $M_s = 800$ kA/m and $A = 10$ pJ/m, respectively. A thin ferromagnetic strip is considered, characterized by a width w and thickness $d = 1$ nm, while the width of the HM strip is denoted by w_D, as illustrated in Fig. 1. To ensure the convergence of the results, the ferromagnetic nanostructure is divided into N sub-strips of width $b = 2$ nm.

Backward volume configuration

The spin-wave dispersion for BV geometry is illustrated in Fig. 2 for the cases $D = 0$ and $D = 1$ mJ/m^2, considering $w = w_D = 100$ nm. The magnitude of the DMI strength (D) is in concordance with values measured experimentally in $Ni_{80}Fe_{20}$/Pt thin films [53]. In Figs. 2(a–d), the SW dispersion (a) and spatial dependence of m_y (b–d) exhibit the expected symmetric bandstructure and the standing modes, respectively. Upon the inclusion of the DM interaction [as depicted in Figs. 2(e–h)], the symmetric nature of the wave dispersion is preserved, but the modes exhibit a nontrivial confinement behavior. This finding is in concordance with earlier studies, [54–56] which have theoretically identified an unusual characteristic of confined waves when DMI is present. Micromagnetic simulations validate the calculated results, as evidenced by the grayscale results in Figs. 2(a) and (e), where an excellent agreement is observed between both methods. The simulated spatial dependence of the low-frequency mode, depicted in Fig. 2(i), is also consistent with the theoretical calculations [see Fig. 2(f)]. Here, the magnetization profiles are excited with a frequency $f_0 = 9.625$ GHz, which allows for exciting the low-frequency mode for $k = \pm 10$ rad/μm. In concordance with chiral magnonic crystals composed by an FM layer in contact with heavy-metal strips periodically distributed [54,57–59], the modes exhibit a certain degree of inclination of the amplitude of the magnetization oscillations that depends on the wave-vector direction. It is worth mentioning that, overall, the frequency of the modes depends on the strip width w, with the mode frequencies decreasing as w increases. Under the influence of DMI, the SW profiles exhibit tilted wave fronts, which perceive a wider geometric confinement compared

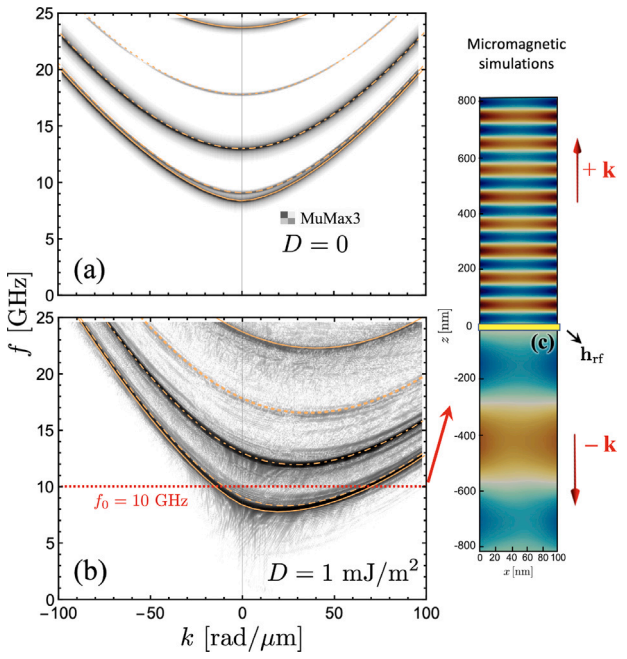

Fig. 4. (a) shows the spin-wave dispersion for the DE modes at $D = 0$. (b) depicts the SW dispersion evaluated at $D = 1$ mJ/m^2. In both cases $w_D = w$. In (a) and (b), the lines correspond to the SW dispersion obtained from the DMM, while the grayscale corresponds to the simulated results. (c) illustrates the simulated SW profiles evaluated at $f_0 = 10$ GHz and $D = 1$ mJ/m^2.

to waves at $D = 0$. As shown in Figs. 2(b) and 2(f), the width of the standing waves at zero DMI corresponds to the strip width w, whereas at $D = 1$ mJ/m^2, the waves are confined within an effective width w_{eff}. Since $w_{\text{eff}} > w$, it is expected that the frequency of the waves under DMI is lower than that at $D = 0$, thus explaining the reduction in frequency of the spin waves in the BV configuration. On the other hand, in the case $D < 0$, the tilted wavefronts for positive wave vectors will resemble those for $-\mathbf{k}$ in Fig. 2(i). In other words, a negative DM constant is equivalent to placing the heavy metal on the bottom face of the ferromagnetic strip.

If the HM layer partially covers the ferromagnetic strip ($w_D < w$), leaving the HM material centered on the FM strip, the modes also reduce their frequencies but with less intensity than in the FM strip fully covered by an HM layer. This effect is expected due to the reduced average DMI along the strip width. This is shown in Fig. 3(a), where the parameters $D = 1$ mJ/m^2, $w = 100$ nm, and $w_D = 0.4w$ have been used. In Figs. 3(b)–(d), the spatial distribution of the dynamic magnetization component m_y presents a striking behavior: It is observed that this magnetization component shows a hybridized localization, where the SW excitation within the zone with HM behaves differently from the zones without DMI although the spins are connected through the exchange in the whole width. For instance, the low-frequency mode (circle) in Fig. 3(b) shows that the waves underneath the HM strip have a spatial dependence similar to the case in Fig. 2(f), while in the regions without DMI, the waves exhibit the typical standing character obtained in Fig. 2(b). The localization behavior observed in Figs. 3(b)–(d), together with the reduction of the SW frequency due to the DM interaction, suggests that it is possible to channel the spin waves in the backward volume configuration. This behavior is further illustrated in Fig. 3(e), where, under a stronger DM interaction of $D = 2$ mJ/m^2, the low-frequency mode is mainly located below the HM strip. For the second low-frequency mode [see Fig. 3(f)], a similar degree of localization is observed, but with excitation across the entire strip width. The micromagnetic simulations conducted for the cases illustrated in Figs. 3(e) and 3(f) are shown in Figs. 3(g) and 3(h), respectively. Here, it can be seen that there is an excellent agreement between both methods, confirming the theoretical predictions and demonstrating the robustness of the dynamic matrix method in capturing the essential features of spin-wave dynamics in the strip systems with DMI. The simulations [Figs. 3(g) and 3(h)] clearly demonstrate that the two counterpropagating waves exhibit distinct characteristics, resulting in nonreciprocal spin-wave channeling. This directional channeling of spin waves, induced by the heavy-metal strip in the backward volume configuration, is a crucial feature with promising applications. These channeled waves can function as *wires* for information transmission without Joule heating, as there is no electron transport, unlike in conventional electronic devices. Thus, these results present an exciting pathway toward energy-efficient nanotechnologies.

Damon–Eshbach configuration

The study now focuses on the Damon–Eshbach configuration, where the equilibrium magnetization is oriented along the strip width (x-axis), as shown in Fig. 1(b). As can be anticipated from Fig. 1, the standing waves in this configuration have the typical node distribution along the strip's width. At the same time, the SW dispersion is asymmetric with respect to the wave vector sign. This behavior is shown in Fig. 4, where the cases $D = 0$ and $D = 1$ mJ/m^2 are illustrated. In Fig. 4(a), the SW dispersion is reciprocal, so that two counterpropagating waves have the same dynamical energy under the inversion of the wave vector. The two low-frequency branches are almost degenerate in frequency and correspond to the edge modes (modes EM1 and EM2 discussed in Ref. [9]). Under the influence of the DMI, all modes become nonreciprocal, as seen in Fig. 4(b), while the modes evaluated at $k = 0$ remain equal for $D = 0$ and $D = 1$ mJ/m^2 but their group velocities change significantly. This behavior is similar to the one observed in an FM thin film coupled with an extended HM layer [12,14]. From Fig. 4(b), it is clear that under excitation of a given frequency f_0, the modes will propagate with different wavelengths, as illustrated in Fig. 4(c). Here, micromagnetic simulations are conducted for $f_0 = 10$ GHz, $D = 1$ mJ/m^2, and a homogeneous excitation $\mathbf{h}_{\text{rf}}$ has been used so that the symmetric (with respect to the strip width center) mode is excited. Due to the strip width ($w = 100$ nm), the edge nature of the mode is not clearly observed because they are distributed over the whole width. Nevertheless, as the strip becomes wider, such modes are more and more localized at the strip edges. Overall, the dynamic behavior of the magnetization in a heavy-metal/FM strip nanostructure is similar to that in an infinite thin film regarding nonreciprocity. However, in the case of the strip, several modes associated with the geometrical confinement are also observed.

Now, the case with $w_D < w$ is studied in the DE geometry. In Fig. 5, the evolution of the modes as a function of w_D and w is shown, when the DM constant is $D = 2$ mJ/m^2. For the case $w_D = 0.1w$ and $w = 100$ nm [see Fig. 5(a)], it is observed that most of the modes tend to be nonreciprocal. This behavior is related to the reduced width w, for which all lateral confined SW modes have a finite SW oscillation amplitude in the zone where the DMI is active, thus having an asymmetric spin-wave dispersion. In contrast, as the width of the FM film increases, as shown in Figs. 5(b)–(c), the nonreciprocal behavior is notable in one [Figs. 5(b)] and two [Figs. 5(c)] modes for the frequency range 0–24 GHz. This effect is associated with the fact that only some modes have a significant SW amplitude in the strip's center, where the HM is in contact with the ferromagnet. Thus, only these modes will be notably nonreciprocal. On the contrary, the rest of the modes have a negligible asymmetry in the SW dispersion because they do not have a significant amplitude of magnetization oscillation at the HM/FM region (not shown). Additionally, as the width w increases, the nonreciprocal modes become increasingly uncoupled from the other modes, as shown in the shaded circles in Figs. 5(a)–(c). Here, the band structure presents a variable anti-crossing effect that indicates the degree of coupling between modes. For a large ferromagnetic width, the nonreciprocal modes do not couple with the reciprocal ones, as

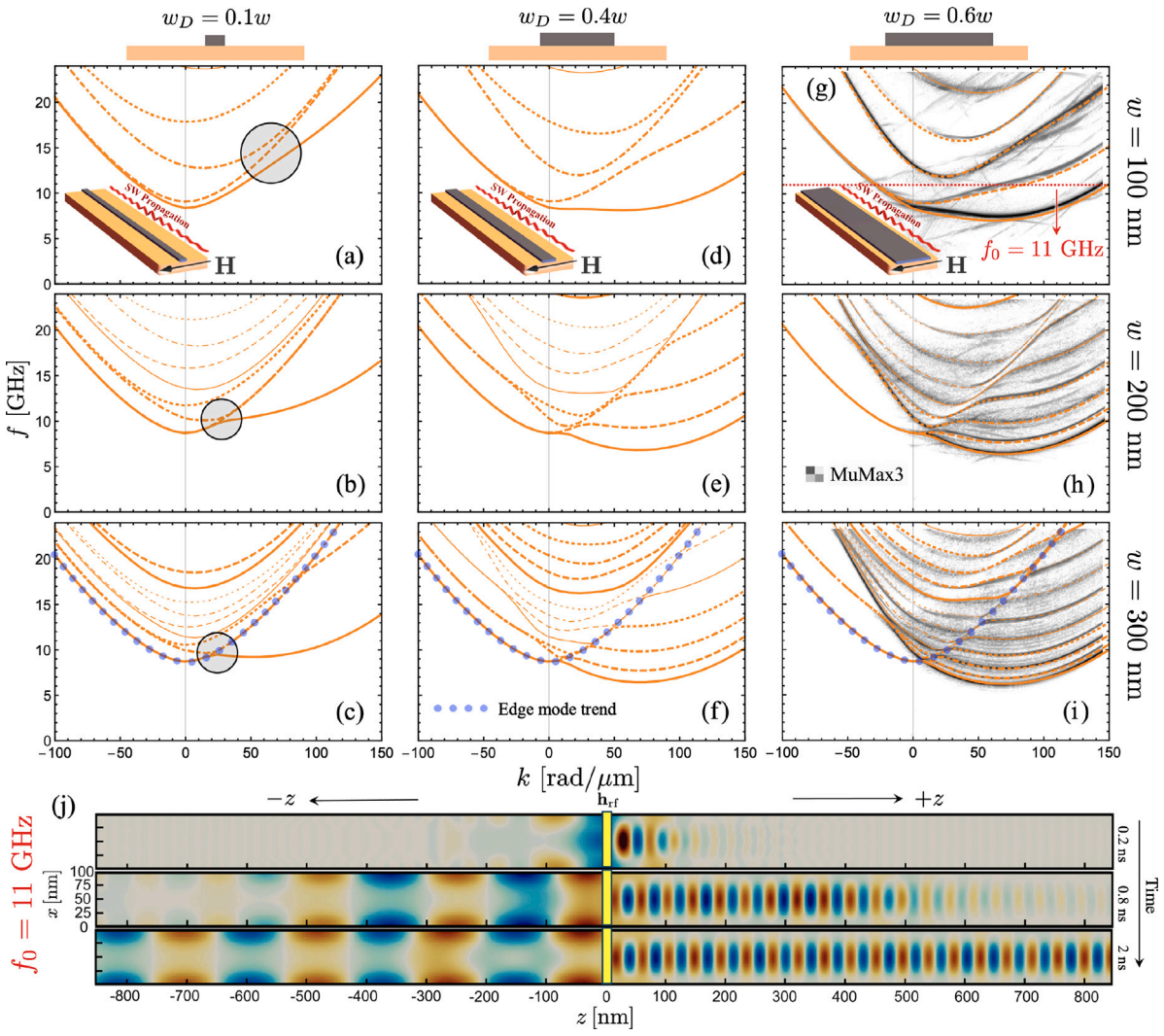

Fig. 5. Spin-wave dispersion evaluated for $w = 100$ nm, 200 nm, and 300 nm (top to bottom). Panels (a), (b), and (c) depict calculations for $w_D/w = 0.1$; (d), (e), and (f) show results for $w_D/w = 0.4$; and (g), (h), and (i) for $w_D/w = 0.6$, respectively. In panels (a) to (c), the shaded circles highlight the coupling between the low-frequency nonreciprocal mode and the symmetric branches. In (c), (f) and (i) the dots highlight the edge mode trend, which has a parabolic reciprocal dispersion. The lines in (a–i) correspond to DMM calculations, while the grayscale in (g) to (i) corresponds to micromagnetic simulations. (j) illustrates the simulated spin waves for case (g) and $f_0 = 11$ GHz, showing unidirectional propagation of the edge modes along the $-z$ direction. The simulations are shown for $t = 0.2$ ns, 0.8 ns and 2 ns.

illustrated in the shaded circle of Fig. 5(c). Hence, the nonreciprocal and reciprocal bands almost intersect in the SW dispersion.

As the ratio between the widths (w_D/w) increases, the nonreciprocity becomes more prominent. This is expected because the averaged DMI along the width increases. This trend is observed in Figs. 5(d)–(i). Most of the modes exhibit an asymmetric SW dispersion, except for those with a parabolic symmetric dispersion that has a minimum frequency at zero wave vector. These modes are precisely the edge modes, characterized by a finite amplitude of magnetization oscillations at the lateral strip edges [9]. Because the DMI is null at the strip edges, these modes behave reciprocally. This effect is highlighted in Figs. 5(c), 5(f) and 5(i), where the dots follow the edge mode trend. As the width of the ferromagnetic strip increases (as seen in the cases for $w = 200$ nm and $w = 300$ nm), the parabolic symmetric behavior of the edge modes becomes more evident due to the uncoupling of the edge and bulk modes. Micromagnetic simulations were performed for the case $w_D = 0.6w$ to validate these results, as shown in Figs. 5(g)–(i). Here, the lines correspond to the calculations, and the gray color represents the simulations. As observed, there is excellent agreement between both methods.

Finally, micromagnetic simulations are used to study the propagation of waves for the case illustrated in Fig. 5(g), where an excitation of $f_0 = 11$ GHz has been applied. As shown in the dispersion relation, at this frequency, modes propagating in the $-z$ direction correspond to an edge mode, while the DMI influences bulk modes in the $+z$ direction. The propagation of the spin waves is depicted in Fig. 5(j) at different times. Here, the unidirectional propagation for the edge and bulk modes is shown. For the simulations realized in Fig. 5(j), a symmetric excitation was used ($\mathcal{A}(x) = 1$, see Section f) so that only the symmetric modes were excited. In the case of the wave propagation along $+z$, such a mode correspond to the one evaluated at $k \sim 150$ rad/μm. It can be observed that the propagation of the bulk mode ($+z$) depends on the size of the HM strip, where the DMI interaction is active, resulting in a robust wave channeling. Thus, the interplay between geometrical parameters and DMI is crucial for controlling the nonreciprocal and unidirectional behavior of spin waves. By fine-tuning the width of the FM strip and the coverage of the HM layer, it is possible to selectively achieve nonreciprocal, unidirectional, and channeled propagation for specific modes, which is essential for designing advanced magnonic devices such as the magnonic diode [36,41], which exploits spin-wave nonreciprocity in a manner similar to an electronic diode, permitting unidirectional propagation of spin-wave signals in magnetic materials. This characteristic is invaluable in developing magnonic devices for

information processing, where control over spin-wave flow direction is essential [60,61].

Summary and conclusions

The spin-wave dynamics in magnetic strips with Dzyaloshinskii–Moriya interaction have been studied in both backward volume and Damon–Eshbach configurations. In the backward volume geometry, the spin-wave dispersion and spatial dependence of the magnetization demonstrate that introducing DMI maintains the symmetric nature of the wave dispersion but alters the lateral confinement of the spin waves. When the heavy-metal layer partially covers the ferromagnetic strip, the spin-wave dispersion remains reciprocal, but the dynamic magnetization component exhibits hybridized localization, differing within the heavy-metal-covered zones compared to the non-DMI zones. This suggests that spin waves can be nonreciprocally channeled in the backward volume configuration, as further corroborated by micromagnetic simulations. In the Damon–Eshbach configuration, where the equilibrium magnetization is oriented along the strip width, spin-wave dispersion becomes asymmetric with the inclusion of DMI, demonstrating nonreciprocal behavior and significant changes in group velocity. Micromagnetic simulations validate these results, showing that nonreciprocal and unidirectional propagation can be controlled by adjusting the geometrical parameters and DMI coverage. This research highlights the potential for designing advanced magnonic devices by exploiting the unique properties of nonreciprocal spin waves, enabling precise control over spin-wave propagation for innovative applications in low-power, high-speed information processing technologies.

CRediT authorship contribution statement

R.A. Gallardo: Writing – original draft, Methodology, Conceptualization. **P. Alvarado-Seguel:** Methodology. **F. Brevis:** Methodology. **C. Gonzalez-Fuentes:** Writing – review & editing. **J.W. González:** Writing – review & editing. **K. Lenz:** Writing – review & editing. **J. Lindner:** Writing – review & editing. **A. Roldán-Molina:** Conceptualization.

Declaration of competing interest

The authors declare that they have no known competing financial interests or personal relationships that could have appeared to influence the work reported in this paper.

Acknowledgments

The authors acknowledge financial support from Fondecyt Grants 1210607, 11220854, 1220700 and 1221301. F.B. acknowledges ANID PhD through Fellowship No. 2021-21211469.

Appendix. Effective DMI field for BV waves

For the backward volume configuration, where the equilibrium magnetization and the SW propagation are along z, the Dzyaloshinskii–Moriya energy density (energy per unit of length) of the ith element can be written as

$$\eta_i^{\mathrm{DM}} = \sum_{\langle j \rangle} \frac{\mathbf{D}_{i,j}^{\mathrm{IS}}}{M_s^2} \cdot (\mathbf{m}_i \times \mathbf{m}_j), \tag{A.1}$$

$$\eta_i^{\mathrm{DM}} = \frac{\mathbf{D}^{\mathrm{IS}}}{M_s^2} \cdot (\mathbf{m}_i \times \mathbf{m}_{i+1} - \mathbf{m}_i \times \mathbf{m}_{i-1}), \tag{A.2}$$

where M_s is the saturation magnetization and $\mathbf{D}_{i,j}^{\mathrm{IS}}$ is the inter-strip (IS) Dzyaloshinskii–Moriya vector, which couples the magnetizations $\mathbf{m}_i$ and $\mathbf{m}_j$. Thus, the dynamic effective DM field acting in the ith sub-strip is

$$\mathbf{h}_i^{\mathrm{IS}} = -\frac{1}{\mu_0 bd} \frac{\partial \eta_i^{\mathrm{DM}}}{\partial \mathbf{m}_i}, \tag{A.3}$$

$$\mathbf{h}_i^{\mathrm{IS}} = -\frac{1}{\mu_0 M_s^2 bd} \left(\mathbf{m}_{i+1} \times \mathbf{D}^{\mathrm{IS}} - \mathbf{m}_{i-1} \times \mathbf{D}^{\mathrm{IS}} \right). \tag{A.4}$$

Then, a complete analysis requires a connection between $D^{\mathrm{IS}} = |\mathbf{D}^{\mathrm{IS}}|$ and D, where this last term is the typical DM constant defined in the continuous approach [13,14,48]. To do this, it is considered that the strip system of width w is divided into many sub-strips of width b. Then, by considering a continuous variation of the DM interaction along x, Eq. (A.2) becomes

$$\eta_i^{\mathrm{DM}} = \frac{\mathbf{D}^{\mathrm{IS}} b}{M_s^2} \cdot \left(\mathbf{m}_i \times \frac{\partial \mathbf{m}_i}{\partial x} \right), \tag{A.5}$$

where the total energy is

$$\eta^{\mathrm{DM}} = \int dS \frac{\mathbf{D}^{\mathrm{IS}}}{M_s^2 d} \cdot \left(\mathbf{m}_i \times \frac{\partial \mathbf{m}_i}{\partial x} \right). \tag{A.6}$$

Here, d is the strip thickness and dS represents a differential element of the transversal section of the sub-strip. Now, for the backward volume configuration illustrated in Fig. 1, the dynamic magnetization can be written as $\mathbf{m}_i = m_x^{(i)} \hat{x} + m_y^{(i)} \hat{y}$. Thus, by considering the interfacial nature of the DMI, namely $\mathbf{D}_{i,j}^{\mathrm{IS}} \perp (\mathbf{r}_j - \mathbf{r}_i)$ ($\mathbf{D}_{i,j}^{\mathrm{IS}} = D^{\mathrm{IS}} \hat{z}$), Eq. (A.6) becomes

$$\eta^{\mathrm{DM}} = \int dS \frac{D^{\mathrm{IS}}}{M_s^2 d} \left(m_x^{(i)} \frac{\partial m_y^{(i)}}{\partial x} - m_y^{(i)} \frac{\partial m_x^{(i)}}{\partial x} \right). \tag{A.7}$$

By comparing Eq. (A.7) with Eq. (1) of Ref. [48], it can be concluded that $D^{\mathrm{IS}} = Dd$, where d is the strip thickness and D is the well-known DM constant, which is energy per area units. Therefore, if the strip system is divided into many sub-strips, there will be a continuous variation of the dynamic magnetization along the strip width so that the constant D^{IS} can be replaced by Dd. Note that in the case when only a few interacting strips are considered, the relation $D^{\mathrm{IS}} = Dd$ is not valid. In this work, a minimum strip width of 100 nm is assumed, where the sub-strip width will be 2 nm, so that the relation $D^{\mathrm{IS}} = Dd$ can be used. Finally, from Eq. (A.4), the dynamic effective field components acting in the ith strip are

$$\left(h_x^{\mathrm{IS}}\right)_i = \frac{D}{\mu_0 M_s^2 b} \sum_\nu m_y^{(\nu)} \left(\delta_\nu^{i+1} - \delta_\nu^{i-1} \right), \tag{A.8}$$

and

$$\left(h_y^{\mathrm{IS}}\right)_i = -\frac{D}{\mu_0 M_s^2 b} \sum_\nu m_x^{(\nu)} \left(\delta_\nu^{i+1} - \delta_\nu^{i-1} \right), \tag{A.9}$$

where δ_j^i stands for the Kronecker delta symbol.

Data availability

Data will be made available on request.

References

[1] Wagner K, Kákay A, Schultheiss K, Henschke A, Sebastian T, Schultheiss H. Magnetic domain walls as reconfigurable spin-wave nanochannels. Nat Nanotechnol 2016;11(5):432–6. http://dx.doi.org/10.1038/nnano.2015.339.

[2] Sluka V, Schneider T, Gallardo RA, Kákay A, Weigand M, Warnatz T, et al. Emission and propagation of 1d and 2d spin waves with nanoscale wavelengths in anisotropic spin textures. Nat Nanotechnol 2019;14(4):328–33. http://dx.doi.org/10.1038/s41565-019-0383-4.

[3] Csaba G, Papp Ádám, Porod W. Perspectives of using spin waves for computing and signal processing. Phys Lett A 2017;381(17):1471–6. http://dx.doi.org/10.1016/j.physleta.2017.02.042, URL https://www.sciencedirect.com/science/article/pii/S0375960116316486.

[4] Nikitov SA, Safin AR, Kalyabin DV, Sadovnikov AV, Beginin EN, Logunov MV, et al. Dielectric magnonics: from gigahertz to terahertz. Phys-Usp 2020;63(10):945. http://dx.doi.org/10.3367/UFNe.2019.07.038609.

[5] Garcia-Sanchez F, Borys P, Vansteenkiste A, Kim J-V, Stamps RL. Nonreciprocal spin-wave channeling along textures driven by the Dzyaloshinskii-Moriya interaction. Phys Rev B 2014;89:224408. http://dx.doi.org/10.1103/PhysRevB.89.224408, URL https://link.aps.org/doi/10.1103/PhysRevB.89.224408.

[6] Henry Y, Stoeffler D, Kim J-V, Bailleul M. Unidirectional spin-wave channeling along magnetic domain walls of bloch type. Phys Rev B 2019;100:024416. http://dx.doi.org/10.1103/PhysRevB.100.024416, URL https://link.aps.org/doi/10.1103/PhysRevB.100.024416.

[7] Liang X, Wang Z, Yan P, Zhou Y. Nonreciprocal spin waves in ferrimagnetic domain-wall channels. Phys Rev B 2022;106:224413. http://dx.doi.org/10.1103/PhysRevB.106.224413, URL https://link.aps.org/doi/10.1103/PhysRevB.106.224413.

[8] Gallardo RA, Alvarado-Seguel P, Schneider T, Gonzalez-Fuentes C, Roldán-Molina A, Lenz K, et al. Spin-wave non-reciprocity in magnetization-graded ferromagnetic films. New J Phys 2019;21(3):033026. http://dx.doi.org/10.1088/1367-2630/ab0449.

[9] Gallardo RA, Alvarado-Seguel P, Brevis F, Roldán-Molina A, Lenz K, Lindner J, et al. Spin-wave channeling in magnetization-graded nanostrips. Nanomaterials 2022;12(16). http://dx.doi.org/10.3390/nano12162785, URL https://www.mdpi.com/2079-4991/12/16/2785.

[10] Jamali M, Kwon JH, Seo S-M, Lee K-J, Yang H. Spin wave nonreciprocity for logic device applications. Sci Rep 2013;3:3160. http://dx.doi.org/10.1038/srep03160.

[11] Barman A, Gubbiotti G, Ladak S, Adeyeye AO, Krawczyk M, Gräfe J, et al. The 2021 magnonics roadmap. J Phys: Condens Matter 2021;33(41):413001.

[12] Cortés-Ortuño D, Landeros P. Influence of the Dzyaloshinskii–Moriya interaction on the spin-wave spectra of thin films. J Phys: Condens Matter 2013;25(15):156001.

[13] Moon J-H, Seo S-M, Lee K-J, Kim K-W, Ryu J, Lee H-W, et al. Spin-wave propagation in the presence of interfacial Dzyaloshinskii-Moriya interaction. Phys Rev B 2013;88:184404. http://dx.doi.org/10.1103/PhysRevB.88.184404, URL http://link.aps.org/doi/10.1103/PhysRevB.88.184404.

[14] Cho J, Kim N-H, Lee S, Kim J-S, Lavrijsen R, Solignac A, et al. Thickness dependence of the interfacial Dzyaloshinskii-Moriya interaction in inversion symmetry broken systems. Nature Commun 2015;6. http://dx.doi.org/10.1038/ncomms8635.

[15] Moriya T. New mechanism of anisotropic superexchange interaction. Phys Rev Lett 1960;4:228–30.

[16] Dzyaloshinsky I. A thermodynamic theory of weak ferromagnetism of antiferromagnetics. J Phys Chem Solids 1958;4(4):241–55.

[17] Fert A, Levy PM. Role of anisotropic exchange interactions in determining the properties of spin-glasses. Phys Rev Lett 1980;44:1538–41.

[18] Seki S, Okamura Y, Kondou K, Shibata K, Kubota M, Takagi R, et al. Magnetochiral nonreciprocity of volume spin wave propagation in chiral-lattice ferromagnets. Phys Rev B 2016;93:235131. http://dx.doi.org/10.1103/PhysRevB.93.235131, URL https://link.aps.org/doi/10.1103/PhysRevB.93.235131.

[19] Crépieux A, Lacroix C. Dzyaloshinsky–Moriya interactions induced by symmetry breaking at a surface. J Magn Magn Mater 1998;182(3):341–9.

[20] Garst M, Waizner J, Grundler D. Collective spin excitations of helices and magnetic skyrmions: review and perspectives of magnonics in non-centrosymmetric magnets. J Phys D: Appl Phys 2017;50(29):293002. http://dx.doi.org/10.1088/1361-6463/aa7573.

[21] Zakeri K, Zhang Y, Prokop J, Chuang T-H, Sakr N, Tang WX, et al. Asymmetric spin-wave dispersion on Fe(110): Direct evidence of the Dzyaloshinskii-Moriya interaction. Phys Rev Lett 2010;104:137203. http://dx.doi.org/10.1103/PhysRevLett.104.137203, URL http://link.aps.org/doi/10.1103/PhysRevLett.104.137203.

[22] Sampaio J, Cros V, Rohart S, Thiaville A, Fert A. Nucleation, stability and current-induced motion of isolated magnetic skyrmions in nanostructures. Nat Nano 2013;8(11):839–44. http://dx.doi.org/10.1038/nnano.2013.210.

[23] Tacchi S, Troncoso RE, Ahlberg M, Gubbiotti G, Madami M, Åkerman J, et al. Interfacial Dzyaloshinskii-Moriya interaction in Pt/CoFeB films: Effect of the heavy-metal thickness. Phys Rev Lett 2017;118:147201. http://dx.doi.org/10.1103/PhysRevLett.118.147201, URL https://link.aps.org/doi/10.1103/PhysRevLett.118.147201.

[24] Melcher RL. Linear contribution to spatial dispersion in the spin-wave spectrum of ferromagnets. Phys Rev Lett 1973;30:125–8.

[25] Kataoka M. Spin waves in systems with long period helical spin density waves due to the antisymmetric and symmetric exchange interactions. J Phys Soc Japan 1987;56(10):3635–47. http://dx.doi.org/10.1143/JPSJ.56.3635.

[26] Otálora JA, Yan M, Schultheiss H, Hertel R, Kákay A. Curvature-induced asymmetric spin-wave dispersion. Phys Rev Lett 2016;117:227203. http://dx.doi.org/10.1103/PhysRevLett.117.227203, URL https://link.aps.org/doi/10.1103/PhysRevLett.117.227203.

[27] Sheka DD, Pylypovskyi OV, Landeros P, Gaididei Y, Kákay A, Makarov D. Nonlocal chiral symmetry breaking in curvilinear magnetic shells. Commun Phys 2020;3(1):128. http://dx.doi.org/10.1038/s42005-020-0387-2.

[28] Gallardo RA, Alvarado-Seguel P, Landeros P. High spin-wave asymmetry and emergence of radial standing modes in thick ferromagnetic nanotubes. Phys Rev B 2022;105:104435. http://dx.doi.org/10.1103/PhysRevB.105.104435, URL https://link.aps.org/doi/10.1103/PhysRevB.105.104435.

[29] Mika K, Grünberg P. Dipolar spin-wave modes of a ferromagnetic multilayer with alternating directions of magnetization. Phys Rev B 1985;31:4465–71. http://dx.doi.org/10.1103/PhysRevB.31.4465, URL https://link.aps.org/doi/10.1103/PhysRevB.31.4465.

[30] Grünberg P, Schreiber R, Pang Y, Brodsky MB, Sowers H. Layered magnetic structures: Evidence for antiferromagnetic coupling of fe layers across cr interlayers. Phys Rev Lett 1986;57:2442–5. http://dx.doi.org/10.1103/PhysRevLett.57.2442, URL https://link.aps.org/doi/10.1103/PhysRevLett.57.2442.

[31] Zhang PX, Zinn W. Spin-wave modes in antiparallel magnetized ferromagnetic double layers. Phys Rev B 1987;35:5219–25. http://dx.doi.org/10.1103/PhysRevB.35.5219, URL https://link.aps.org/doi/10.1103/PhysRevB.35.5219.

[32] Binasch G, Grünberg P, Saurenbach F, Zinn W. Enhanced magnetoresistance in layered magnetic structures with antiferromagnetic interlayer exchange. Phys Rev B 1989;39:4828–30. http://dx.doi.org/10.1103/PhysRevB.39.4828, URL https://link.aps.org/doi/10.1103/PhysRevB.39.4828.

[33] Barnaś J, Grünberg P. Spin waves in exchange-coupled epitaxial double-layers. J Magn Magn Mater 1989;82(2):186–98. http://dx.doi.org/10.1016/0304-8853(89)90153-4, URL http://www.sciencedirect.com/science/article/pii/0304885389901534.

[34] Gallardo RA, Schneider T, Chaurasiya AK, Oelschlägel A, Arekapudi SSPK, Roldán-Molina A, et al. Reconfigurable spin-wave nonreciprocity induced by dipolar interaction in a coupled ferromagnetic bilayer. Phys Rev Appl 2019;12:034012. http://dx.doi.org/10.1103/PhysRevApplied.12.034012, URL https://link.aps.org/doi/10.1103/PhysRevApplied.12.034012.

[35] Albisetti E, Tacchi S, Silvani R, Scaramuzzi G, Finizio S, Wintz S, et al. Optically inspired nanomagnonics with nonreciprocal spin waves in synthetic antiferromagnets. Adv Mater 2020;32(9):1906439. http://dx.doi.org/10.1002/adma.201906439, URL https://onlinelibrary.wiley.com/doi/abs/10.1002/adma.201906439.

[36] Grassi M, Geilen M, Louis D, Mohseni M, Brächer T, Hehn M, et al. Slow-wave-based nanomagnonic diode. Phys Rev Appl 2020;14:024047. http://dx.doi.org/10.1103/PhysRevApplied.14.024047, URL https://link.aps.org/doi/10.1103/PhysRevApplied.14.024047.

[37] Franco AF, Landeros P. Enhancement of the spin-wave nonreciprocity in antiferromagnetically coupled multilayers with dipolar and interfacial Dzyaloshinskii-Moriya interactions. Phys Rev B 2020;102:184424. http://dx.doi.org/10.1103/PhysRevB.102.184424, URL https://link.aps.org/doi/10.1103/PhysRevB.102.184424.

[38] Gallardo R, Weigand M, Schultheiss K, Kakay A, Mattheis R, Raabe J, et al. Coherent magnons with giant nonreciprocity at nanoscale wavelengths. ACS Nano 2024;18(7):5249–57. http://dx.doi.org/10.1021/acsnano.3c08390.

[39] Di K, Feng SX, Piramanayagam SN, Zhang VL, Lim HS, Ng SC, et al. Enhancement of spin-wave nonreciprocity in magnonic crystals via synthetic antiferromagnetic coupling. Sci Rep 2015;5. http://dx.doi.org/10.1038/srep10153, 10153 EP –.

[40] Alvarado-Seguel P, Gallardo RA. Band structure of a one-dimensional bilayer magnonic crystal. Phys Rev B 2019;100:144415. http://dx.doi.org/10.1103/PhysRevB.100.144415, URL https://link.aps.org/doi/10.1103/PhysRevB.100.144415.

[41] Lan J, Yu W, Wu R, Xiao J. Spin-wave diode. Phys Rev X 2015;5:041049. http://dx.doi.org/10.1103/PhysRevX.5.041049, URL https://link.aps.org/doi/10.1103/PhysRevX.5.041049.

[42] Reiskarimian N, Krishnaswamy H. Magnetic-free non-reciprocity based on staggered commutation. Nature Commun 2016;7:11217. http://dx.doi.org/10.1038/ncomms11217.

[43] Sounas DL, Alù A. Non-reciprocal photonics based on time modulation. Nat Photonics 2017;11(12):774–83. http://dx.doi.org/10.1038/s41566-017-0051-x.

[44] Heussner F, Serga AA, Brächer T, Hillebrands B, Pirro P. A switchable spin-wave signal splitter for magnonic networks. Appl Phys Lett 2017;111(12):122401. http://dx.doi.org/10.1063/1.4987007.

[45] Heussner F, Talmelli G, Geilen M, Heinz B, Brächer T, Meyer T, et al. Experimental realization of a passive gigahertz frequency-division demultiplexer for magnonic logic networks. phys status solidi RRL 14(4):1900695. http://dx.doi.org/10.1002/pssr.201900695, URL https://onlinelibrary.wiley.com/doi/abs/10.1002/pssr.201900695.

[46] Xing X, Zhou Y, Braun H. Magnetic skyrmion tubes as nonplanar magnonic waveguides. Phys Rev Appl 2020;13:034051. http://dx.doi.org/10.1103/PhysRevApplied.13.034051, URL https://link.aps.org/doi/10.1103/PhysRevApplied.13.034051.

[47] Körber L, Verba R, Otálora JA, Kravchuk V, Lindner J, Fassbender J, et al. Curvilinear spin-wave dynamics beyond the thin-shell approximation: Magnetic nanotubes as a case study. Phys Rev B 2022;106:014405. http://dx.doi.org/10.1103/PhysRevB.106.014405, URL https://link.aps.org/doi/10.1103/PhysRevB.106.014405.

[48] Di K, Zhang VL, Lim HS, Ng SC, Kuok MH, Yu J, et al. Direct observation of the Dzyaloshinskii-Moriya interaction in a pt/co/ni film. Phys Rev Lett 2015;114:047201. http://dx.doi.org/10.1103/PhysRevLett.114.047201, URL http://link.aps.org/doi/10.1103/PhysRevLett.114.047201.

[49] Vansteenkiste A, Leliaert J, Dvornik M, Helsen M, Garcia-Sanchez F, Van Waeyenberge B. The design and verification of Mumax3. AIP Adv 2014;4(10):107133. http://dx.doi.org/10.1063/1.4899186.

[50] Mulkers J, Van Waeyenberge B, Milošević MV. Effects of spatially-engineered Dzyaloshinskii-Moriya interaction in ferromagnetic films. Phys Rev B 2017;95(14):144401. http://dx.doi.org/10.1103/PhysRevB.95.144401.

[51] Cortés-Ortuño D. Oommfpy, zenodo. 2019, http://dx.doi.org/10.5281/zenodo.2611194, Github: https://github.com/davidcortesortuno/oommfpy.

[52] Beg M, Lang M, Fangohr H. Ubermag: Toward more effective micromagnetic workflows. IEEE Trans Magn 2022;58(2):1–5. http://dx.doi.org/10.1109/TMAG.2021.3078896.

[53] Nembach HT, Shaw JM, Weiler M, Jué E, Silva TJ. Linear relation between heisenberg exchange and interfacial Dzyaloshinskii–Moriya interaction in metal films. Nat Phys 2015;11(10):825–9. http://dx.doi.org/10.1038/nphys3418.

[54] Gallardo RA, Cortés-Ortuño D, Schneider T, Roldán-Molina A, Ma F, Troncoso RE, et al. Flat bands, indirect gaps, and unconventional spin-wave behavior induced by a periodic Dzyaloshinskii-Moriya interaction. Phys Rev Lett 2019;122:067204. http://dx.doi.org/10.1103/PhysRevLett.122.067204, URL https://link.aps.org/doi/10.1103/PhysRevLett.122.067204.

[55] Zingsem BW, Farle M, Stamps RL, Camley RE. Unusual nature of confined modes in a chiral system: Directional transport in standing waves. Phys Rev B 2019;99:214429. http://dx.doi.org/10.1103/PhysRevB.99.214429, URL https://link.aps.org/doi/10.1103/PhysRevB.99.214429.

[56] Silvani R, Alunni M, Tacchi S, Carlotti G. Effect of the interfacial Dzyaloshinskii–Moriya interaction on the spin waves eigenmodes of isolated stripes and dots magnetized in-plane: A micromagnetic study. Appl Sci 2021;11(7).

[57] Flores-Farías J, Gallardo RA, Brevis F, Roldán-Molina A, Cortés-Ortuño D, Landeros P. Omnidirectional flat bands in chiral magnonic crystals. Sci Rep 2022;12(1):17831. http://dx.doi.org/10.1038/s41598-022-20539-3.

[58] Tacchi S, Flores-Farías J, Petti D, Brevis F, Cattoni A, Scaramuzzi G, et al. Experimental observation of flat bands in one-dimensional chiral magnonic crystals. Nano Lett 2023;23(14):6776–83. http://dx.doi.org/10.1021/acs.nanolett.2c04215.

[59] Flores-Farías J, Cortés-Ortuño D, Brevis F, Landeros P, Gallardo RA. Selective nonreciprocal localization of flat magnonic modes induced by a periodic Dzyaloshinskii-Moriya interaction. Phys Rev B 2024;109:054423. http://dx.doi.org/10.1103/PhysRevB.109.054423, URL https://link.aps.org/doi/10.1103/PhysRevB.109.054423.

[60] Sadovnikov AV, Beginin EN, Odincov SA, Sheshukova SE, Sharaevskii YP, Stognij AI, et al. Frequency selective tunable spin wave channeling in the magnonic network. Appl Phys Lett 2016;108(17):172411. http://dx.doi.org/10.1063/1.4948381.

[61] Roberjot P, Szulc K, Kłos JW, Krawczyk M. Multifunctional operation of the double-layer ferromagnetic structure coupled by a rectangular nanoresonator. Appl Phys Lett 2021;118(18):182406. http://dx.doi.org/10.1063/5.0046001.